CLOSED-LOOP BLADDER FUNCTION CONTROL FOR RATS USING OPTOGENETICS

BY

KYUNG NIM NOH

THESIS

Submitted in partial fulfillment of the requirements
for the degree of Master of Science in Electrical and Computer Engineering
in the Graduate College of the
University of Illinois at Urbana-Champaign, 2017

Urbana, Illinois

Adviser:

Professor John A. Rogers

ABSTRACT

Implantable devices are continuously proving to be an effective and reliable method of treatment for human patients in clinical settings. One example class of these devices is closed-loop or conditional-triggering implantable devices, which monitor physiological signals and provide necessary intervention only when necessary. Pacemakers are one of the most widely used conditional stimulating devices that continuously monitor the heart activity and electrically stimulate the heart only when abnormal conditions are detected. This thesis presents a closed-loop bladder function control system for rats. The bladder activity is monitored using a novel sensor in a less invasive manner than the traditional pressure sensors. A neuromodulation technique called optogenetics is used as the method of intervention to help control the bladder function. The battery-less implantable device is wirelessly powered via inductive resonance coupling to reduce the size of the implantable device by eliminating batteries and charging circuits. A custom-built iOS application monitors the bladder activity for abnormal behavior and triggers neuromodulation by sending a signal to the implanted device. *In vivo* experiments with rats demonstrate the feasibility of closed-loop implantable devices to modulate bladder function and lay the foundations for such implantable devices in clinical settings.

ACKNOWLEDGMENTS

First and foremost, I would like to thank my adviser, Professor John Rogers, for giving me the opportunity to contribute to the research in his group and his guidance throughout my research career. He provided an incredible environment and invaluable resources to pursue all of my research interests that would have not been possible anywhere else.

Second, I would like to thank Professor Sung Il Park for his mentorship in building my research interests. He enabled my potential enthusiasm for research, and thus this work would not have been possible without his support and guidance.

Third, many people in the Rogers Research Group have helped make this work possible. I thank Sang Min Won, Dr. Jangyeol Yoon, Ha Uk Chung, and Dr. Kaitlyn Crawford for assisting me throughout various aspects of the project. I also want to thank the collaborators of the Gereau Lab at Washington University of St. Louis, especially Aaron D. Mickle, for their understanding and allowing this work to potentially impact a larger scientific community in the future.

Finally, I want to thank my family and friends for their unconditional support during this stage of my life. They truly challenge me to become a better person every day.

This research was supported by the Stimulating Peripheral Activity to Relieve Conditions Program by the National Institutes of Health.

TABLE OF CONTENTS

CHAPTER 1: INTRODUCTION

1.1 Implantable Devices

Since the first demonstration of electrical stimulation in a clinical setting in 1952, implantable devices have increasingly become a popular method of treatment. Generally, a medical device is referred to as "implantable" if it is surgically introduced into a living body and remains inside after the procedure. Such invasive introduction of foreign objects into the body is a challenging task requiring careful consideration of various engineering disciplines and medical sciences. Moreover, the risks of surgical complications are always present, but the potential benefits of these devices justify their needs and continuous development [1]. A wide variety of implantable devices exist, ranging from passive devices, such as artificial knees and hips, to more sophisticated systems such as cochlear implants and cardioverter defibrillators. In most cases, these devices need to be implanted to continuously monitor and/or provide treatment for certain organs.

One method to maximize the efficacy of implantable devices is to develop a closed-loop feedback system. The ultimate goal of a closed-loop device is to continuously monitor certain organs or tissues and trigger a method of intervention to improve the organ functionality. A common example is the pacemaker, which is an implantable device that monitors the heart and intervenes by using electrical stimulation when abnormal heart rhythm is detected. Electrical stimulation via electrodes is a conventional method to activate or inhibit neurons

for these devices. While a very extensive understanding of the neural signals and organ function is needed to model such feedback systems, these devices enable a very consistent and reliable control of organ functions outside a clinical setting. This work presents a feedback system to help control bladder function using a novel bladder measurement method and an unconventional neuromodulation technique.

1.2 Bladder Disease

This closed-loop system for rats can provide not only insight into the physiology of bladder function, but also lay out a foundation for developing similar devices for human beings. The most common bladder condition among patients in the United States is called interstitial cystitis (also known as bladder pain syndrome) [2]. Patients with this disease go through a wide range of symptoms and severity, most commonly pain associated with bladder filling and increased urgency and frequency of urination. While the pathogenesis of the disease is not fully understood, there have been successful treatments to reduce pain and alleviate the symptoms, such as electrical stimulation of the sacral nerve [3]. Despite its effectiveness, there are drawbacks to sacral nerve stimulation. Like most electrical stimulation, it is hard to localize, potentially causing off-target side effects. Most importantly, sacral nerve stimulation is performed in a pre-programmed, rather than a conditional, manner which decreases its effectiveness over time. Thus, a spatially localized and conditional stimulation of the bladder function can greatly improve the care of patients suffering from

bladder conditions, and the system presented here attempts to provide a potential alternative to the sacral nerve stimulation with a conditional and spatially localized stimulation of the bladder.

1.3 Overview

This thesis is divided into five chapters that contribute to the development of this system. Chapter 2 discusses the motivations to develop the system, along with potential benefits this study may have in different scientific fields. Chapter 3 explains the development of each component in the implantable device and the closed-loop system. The engineering design choices and tradeoffs are explained in detail in this chapter. Chapter 4 presents the results and discussion of biology experiments conducted with the closed-loop system. Chapter 5 provides a summary of the work presented and provides potential future directions of research. While all the aspects of the system are mentioned, this thesis focuses on system-level design with an emphasis on the electronics.

CHAPTER 2: MOTIVATION AND BENEFITS

2.1 Bladder Band Strain Sensor

Traditional bladder activity measurements utilize pressure transducers to monitor internal bladder pressure. This method applies for both animals and humans alike, with a few other options available for smaller animals such as rats. The two most common methods of studying bladder function in awake, unanesthetized rats utilize either pressure measurement catheters or metabolic cages. Metabolic cages integrate an analytical balance beneath a cage to measure the rats' urination activity. While non-invasive, this method only provides limited information regarding the void volume and frequency. The more invasive, pressure measurement cystometry is conducted by inserting a catheter into the bladder wall which is tunneled subcutaneously to the back of the neck. This method allows direct measurement of intravesicular pressure to offer a better understanding of bladder activity, but requires an incision in the bladder wall which can affect the normal bladder behavior. Additionally, the connection of the catheter to an external system requires a special caging environment for the measurement and limits the rats' movement. Several sensors and wireless measurement methods have been proposed as alternatives for monitoring bladder function, but have been limited to large animal species and also lack *in vivo* experiments [4-7].

The novel bladder band strain sensor presented here attempts to overcome most of the drawbacks associated with the bladder pressure transducers. By employing a biocompatible and flexible strain sensor, a less invasive method is used to monitor the bladder activity. The stretchable strain sensor is horizontally wrapped around the rat's bladder to provide a relative measurement of the bladder's physical dimensions. Because the bladder activity can be interpreted from expansions and contractions of the bladder, monitoring the physical size can be a viable method to understand bladder activity. This eliminates the need for an incision in the bladder wall, making the proposed sensor less invasive. Moreover, when the sensor is connected to an implantable device, the bladder activity can be measured in an awake, unanesthetized rat without the need of a tethered catheter. Figure 2.1 shows pictures of the traditional intravesicular pressure measurement and the novel strain sensor measurement. Details of the strain sensor and its correlation with the pressure measurement are given in subsequent chapters.

2.2 Closed-loop Organ Function Control

As previously mentioned, the main objective of the implantable device is to modulate bladder function depending on acquired physiological signals from the strain sensor. The implantable device transmits the strain sensor measurements to an iPad, which has a custom-built iOS application that recognizes when the bladder is overactive. To alleviate overactive bladder conditions, electrical stimulation of the sacral nerve has proven to be an effective method to decrease the urinating urgency and frequency with constant

stimulation. A more effective method is conditional stimulation, which stimulates only at intervals when the bladder is overactive. Conditional stimulation has been shown to be as effective while mitigating some of the side effects due to constant stimulation [3]. However, a catheter measurement can only be used in a hospital setting with current technology, making it impossible to build an implantable device with transducers. Thus, the proposed strain sensor is not only less invasive, but also opens opportunities for integration with implantable devices that enable monitoring in a non-hospital setting. The system presented here exploits this opportunity to include a neuromodulation technique called optogenetics, which will be described next.

2.3 Optogenetics

The neuromodulation used in this system is a technique called optogenetics, which combines optics and genetics to control genetically modified neurons [8]. Traditional stimulation of nerves incorporates electrical stimulations, which have inevitable side effects. The most common side effect is the non-specific targeting of neurons, which introduces the possibility of off-target nerve activation. Optogenetics, on the other hand, uses genetically encoded light-sensitive channels to modulate neural activity. When neurons are genetically encoded, optics at a certain wavelength trigger neural activity by reacting to photosensitive proteins. This technique enables stimulation of the specific neural population that has been genetically encoded and completely avoids off-target stimulation [8].

For the experiments presented here, optogenetic inhibitory pumps called Archaerhodopsins are used to activate optogenetic proteins. The neuromodulation of the bladder function utilizes a 450 nm (green) light illumination to these encoded neurons, which causes silencing of neural activities. Until recently, most optogenetics experiments were carried out with optical fibers and lasers that were tethered inside the animals, severely limiting their natural behavior. While new studies have just started exploring the possibilities of building miniaturized implantable devices for optogenetic experiments [9], the device presented here incorporates μ-iLEDs with the strain sensor such that it can intimately interface with the genetically encoded region of the bladder. Triggering of the μ-iLEDs with a microcontroller enables high temporal precision that can be either pre-programmed or set using an external device. The integrated μ-iLEDs for optogenetics are shown in the strain sensor in Figure 2.1, and a simplified closed-loop system is illustrated in Figure 2.2.

2.4 Figures

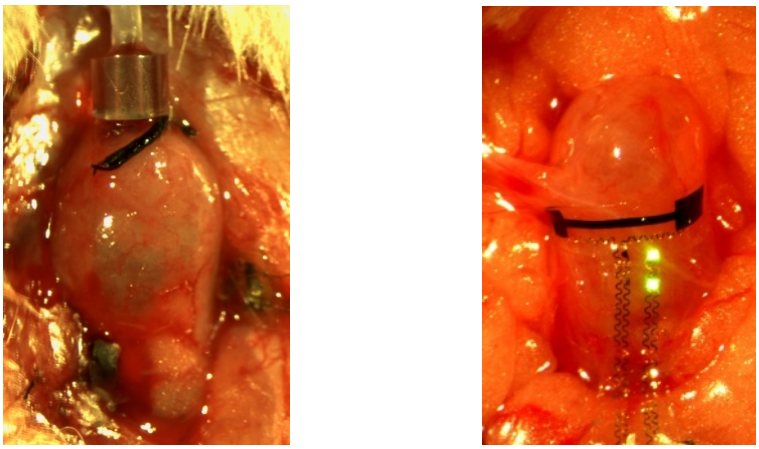

Figure 2.1: Comparison between rat bladder activity measurement using a pressure transducer (left) and strain sensor with integrated μ-iLEDs (right). The transducer is inserted into the bladder wall through an incision, while the strain sensor is wrapped around the bladder, eliminating the need to make an incision.

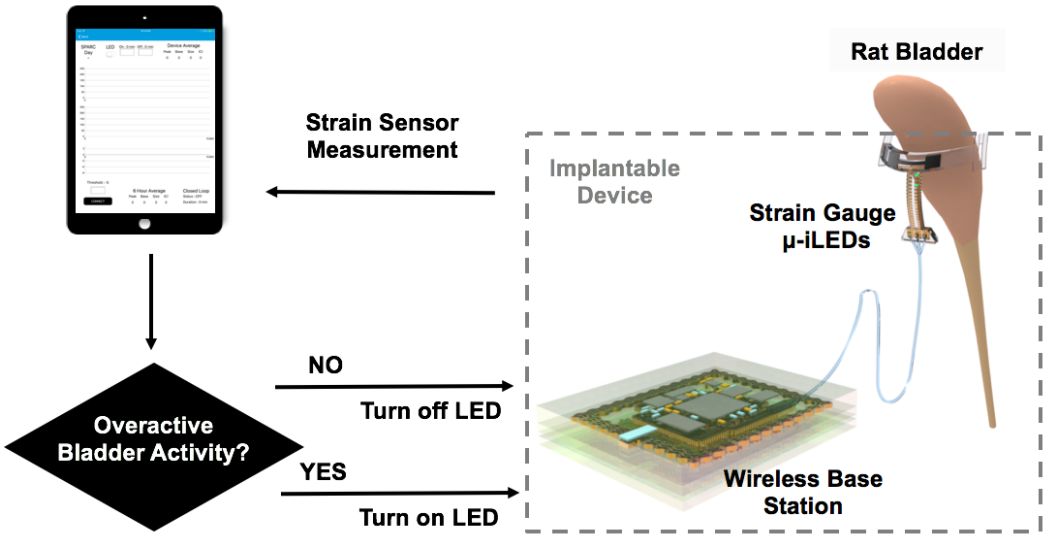

Figure 2.2: Schematic illustration of conditional neuromodulation using μ-iLEDs. The iOS application determines whether bladder activity is abnormal.

CHAPTER 3: DEVELOPMENT

3.1 Overview

The closed-loop system can be divided into four subsystems: strain sensor/μ-iLEDs, powering circuit, Bluetooth controller, and the iOS application software. Figure 3.1 is a block diagram of the system, with components color-coded according to the four subsystems. First, the strain sensor/μ-iLEDs component is designed to safely interface with the bladder and includes the accompanying analog signal conditioning circuitry. Second, the powering circuit includes the components that are required to wirelessly deliver power to the implantable device and is composed of the primary coil driver, primary coil antenna, intermediate resonator, load coil antenna, supercapacitors and the power supply circuitry. Third, the Bluetooth microcontroller functions as the main controller of the implantable device with an embedded Bluetooth stack (S110, Nordic Semiconductor Inc.) that controls the wireless communication. The microcontroller is responsible for acquiring the sensor signals and triggering the μ-iLEDs. The last component is the iOS application which receives measurements from the implantable device and evaluates the bladder activity. When abnormal condition is detected through the software, it sends a signal to the implantable device to trigger the μ-iLEDs, thus closing the loop. Each component is explained in detail in the following sections.

3.2 Integrated Strain Sensor and μ-iLEDs

3.2.1 Strain Sensor

A strain sensor is a piezoresistive device used to measure strain on an object. Traditionally, metal strain sensors (or strain gauge) have been commonly used to measure the applied strain on an object. Due to the piezoresistive nature, when strain is applied on the object, the attached strain sensor deforms, thereby changing the resistance of the strain sensor. By monitoring the resistance of the strain sensor, the strain applied on the external object can be inferred from the properties of the strain sensor material. The gauge factor is an important property of a strain sensor, which characterizes the sensitivity of the device and can be expressed as

$$\mathrm{GF} = \frac{\Delta R/R}{\Delta L/L} = \frac{\Delta R/R}{\varepsilon} \tag{3.1}$$

where R is the original strain gauge resistance, L is the original length of the strain gauge, and ε is the applied strain on the strain gauge along the direction of L. Thus, the gauge factor is the ratio of relative resistance change to the applied mechanical strain, effectively characterizing the resistive sensitivity.

The strain sensor used to monitor bladder activity for this closed loop system is a biocompatible and stretchable strain sensor that is able to detect the relative change of the bladder's physical dimensions. To integrate the strain sensor onto the bladder without constricting its natural movement, the strain

sensor needs to have a modulus close to, or lower than, that of the rat's bladder. Therefore, the substrate of the strain sensor is fabricated on a material called Eco-flex (Ecoflex 00-30, Smooth-On Inc.) which has a low modulus of 60 kPa. Carbon-doped (15%) Eco-flex is embedded inside the substrate in an 8 mm by 300 μm rectangular geometry with a thickness of ~15 μm and acts as the actual piezoresistive sensor as seen in Figure 3.2a. The carbon-doped Eco-flex is patterned with ends coinciding to gold layer pads which are interconnected by serpentine traces to another set of pads where 8 cm 40-gauge wires are connected to the wireless base station of the implantable device as shown in Figure 3.2b.

Mechanical measurements characterizing the strain sensor are plotted in Figure 3.2c-d, where the resulting elastic modulus is ~75 kPa and gauge factor is ~2, representing that the change in relative resistance is ~2 times that of the change in strain. While the change in bladder dimension during contraction and expansion varies significantly among rats and with the exact positioning of the strain sensor, *in vivo* experiments have shown that the change in resistance is roughly 20% of the initial resistance. Moreover, the strain sensor's initial resistance also varies due to imperfections in fabrication, ranging from 300 kΩ to 500 kΩ. Because there is no gold standard in measuring the modulus of the rats' bladder [10], cystometries were conducted on the same rats to verify that the bladder activity was not affected by the strain sensor applied on the bladder.

3.2.2 Sensor Signal Conditioning

A Wheatstone bridge circuit is utilized to measure the resistance of the strain sensor, which corresponds to the relative size of the bladder. The bridge circuit indirectly measures an unknown resistance by comparing it with other known resistances, usually operating in a balanced bridge configuration. The bridge circuit with the strain sensor, including the remaining analog front-end circuit, is shown in Figure 3.3. As seen in the figure, the output of the bridge circuit, V_B, is a differential voltage between two voltage-dividing resistor arms, where one of the four resistors is the strain sensor, R_S. Because the strain sensor lengths were chosen to match the circumference of the empty bladder, the bridge resistances are chosen to match the initial resistance of the strain sensor, effectively nulling the differential voltage when the bladder is emptied. The differential voltage, V_B, with the strain sensor at its initial state can be calculated as

$$V_B = V_{DD} \left(\frac{R_S}{R_S + R_1} - \frac{1}{2} \right) \tag{3.2}$$

As previously mentioned, experiments have shown that the resistance of the strain sensor is initially ~300 kΩ to ~500 kΩ and ~1.2 times the initial resistance when the bladder fully expands. Then the differential voltage, V_B, when strain is applied, assuming R_1 is matched to R_S, can be calculated as

$$V_B = V_{DD}\left(\frac{R_S+\Delta R}{R_S+R_1+\Delta R}-\frac{1}{2}\right)=\frac{V_{DD}}{4}\left(\frac{\Delta R}{R_S+\frac{\Delta R}{2}}\right) \quad (3.3)$$

Due to the ΔR term in the denominator of the right hand side of (3.3), it is important to note that the output voltage is not strictly linear with respect to the strain sensor resistance and has a worst-case non-linearity error of 0.5 %/%. However, it will be shown that such error is negligible due to other sources of error and noise. Evaluating (3.3), the sensitivity and the accuracy of the bridge measurement system are calculated. The sensitivity of the system, which corresponds to the full-range output with 1 V excitation voltage is found in (3.4), assuming initial sensor resistance of 500 kΩ.

$$\text{Sensitivity} = \frac{1}{4}\left(\frac{100\ \text{k}\Omega}{500\ \text{k}\Omega+\frac{100\ \text{k}\Omega}{2}}\right) = 45\ [\text{mv/V}] \quad (3.4)$$

To fully utilize the V_{DD} swing with the strain sensor resistance, the output of the bridge circuit needs to be amplified such that the range of the strain sensor resistance corresponds to the supply voltage for maximum resolution. Since the bridge circuit has a high output impedance (~250 kΩ), a buffer at the input stage of the amplifier is needed for proper loading onto the amplifier. A convenient way to implement the buffer is by using an instrumental amplifier (INA333, Texas Instruments), which has a buffer at both terminals of the input stage. Advantages of using an instrumental amplifier with a bridge circuit include convenient gain modification, high common-mode rejection ratio (~110 dB), low system noise

(~10 nV $\sqrt{\text{Hz}}$), and direct radiometric output [11]. As seen in Figure 3.3, the buffered differential input voltage is applied along R_G, forcing a current flow from V_o to the ground node. Therefore, this resistor effectively sets the gain of the system which is finally passed through an internal unity-gain differential amplifier. Then, the output of the overall amplifier stage can be expressed as

$$V_O = \left(1 + \frac{2 \times 50{,}000}{R_g}\right) \times V_B = \frac{V_{DD}}{4}\left(1 + \frac{2 \times 50{,}000}{R_g}\right)\left(\frac{\Delta R}{R_S + \frac{\Delta R}{2}}\right) \quad (3.5)$$

The gain is set to match the output of the amplifier swing to a resistance range corresponding to the initial sensor resistance to twice its initial resistance. In the example of a 500 kΩ strain sensor, the gain resistor, R_G, is calculated as

$$R_G = \frac{100}{Gain - 1} = \frac{100}{\frac{3}{3 \times Sensitivity} - 1} = 20\ \text{k}\Omega \quad (3.6)$$

for a gain of 6 and a range from 500 kΩ to 1MΩ. This leaves an upper margin in cases the strain sensor is relatively more sensitive or the initial resistance drifts upwards. The instrumental amplifier draws a quiescent current of 50 μA and the bridge circuit consumes 3 μA for a total power consumption of 159 μW in the analog sensor component. Finally, the output of the instrumental amplifier is connected to an analog input of the microcontroller, which utilizes an internal analog-to-digital converter to digitally transmit the strain sensor reading to the iPad.

3.2.3 μ-iLEDs

The μ-iLEDs used to neuromodulate the bladder are embedded in the substrate of the strain sensor to closely interface with the bladder. To ensure activation of the optogenetic proteins, optical density of 1 mW/mm^2 is required at the location of target neurons [12]. As previously shown in Figure 2.1, the outer encapsulation of the strain sensor/μ-iLEDs is physically in contact with the bladder tissue, minimizing absorption and scattering of the optical power in the surrounding tissues. Two commercial μ-iLEDs (C527TR2227-0213, Cree Inc.) are soldered onto the gold pads that are patterned along with the strain sensor pads, and interconnected to the other set of gold pads where the 40-gauge wire is connected. The micro-scaled (220 μm × 270 μm × 50 μm) and low-powered (2 mW turn-on) devices allow miniaturized integration on the strain sensor with minimal power consumption. Although the power consumption is very low with a turn-on voltage of ~2 V , the μ-iLEDs still generate a certain level of heat at the surface, which can distort the bladder's normal activity. To operate the μ-iLEDs at the organ temperature, the temperature at the substrate of the μ-iLEDs should not exceed ~38 °C. In order to find the current that corresponds to this temperature change, temporal temperature measurements are recorded using an IR camera and plotted in Figure 3.4. Measurements indicate that a 2.7 V and 3.3 mA applied on each μ-iLED corresponds to optical density of 50 mW/mm^2 and is thermally safe. Therefore, a current-limiting resistor with a transistor (RUM001, Rohm Semiconductor) is used to set the current to 3.3 mA for each μ-iLED as shown in Figure 3.5.

3.3 Powering Scheme

The implantable device is a battery-less system powered wirelessly using resonant inductive coupling. This enables the device to operate without bulky batteries, allowing virtually infinite device lifetime and further miniaturization of the implantable device. However, resonant inductive coupling has severe drawbacks, such as sensitivity to angle mismatches, antenna dimension mismatches, and antenna separations, necessitating careful system-level design considerations [13]. The overall setup of wireless powering is given in Figure 3.6. As seen in the figure, the base station of the implantable device, which includes the load coil antenna, is subcutaneously implanted near the upper abdomen. Then, placing the primary coil antenna below the cage parallel to the cage floor allows the wireless powering antennas to be parallel to each other most of the time, while also minimizing the variability of the distance between the primary and load antennas. However, the angle between the two might vary if the rat were to stand up, which would significantly decrease the power transfer efficiency. As a countermeasure, supercapacitors are utilized to act as a short-term energy buffer in case of insufficient power delivered during periods of mismatched angles. Therefore, the overall powering scheme integrates wireless power transfer (source driver, primary coil antenna, intermediate resonator, load coil antenna), supercapacitors, and voltage regulating circuitry, which are described next.

3.3.1 Wireless Power Transfer

Ampere's law states that the magnetic field around an area is proportional to the amount of current flowing through the enclosed area, and Faraday's law demonstrates that a varying magnetic flux through a loop conductor induces an electromotive force (EMF) on the conductor. Therefore, when a varying current is driven in a coil, it generates an induced EMF in any coils in the vicinity. These simple electromagnetic laws laid the foundation of non-radiative wireless power transfer using inductive coupling. In inductive coupling, mutual inductance characterizes how much voltage is induced relative to a current excitation on the other coil, and the coupling coefficient is the ratio of flux generated at one coil to the amount of flux flowing through the second coil, which can be expressed as

$$k = \frac{M}{\sqrt{L_1 L_2}} \tag{3.7}$$

where L is the self-inductance of each coil and M is the mutual inductance. The mutual inductance is governed by the geometry and the separation of the coils. Another important characteristic of a coil antenna is the Q factor, which describes how under-damped a coil is, and can be found as

$$Q = \frac{|Z_{Im}|}{Z_{Re}} = \frac{\left|\omega L\left(1-\omega^2 LC-\frac{CR^2}{L}\right)\right|}{R} \tag{3.8}$$

where Z is the impedance and ω is the self-resonant frequency of the coil. The Q factor is an important parameter characterizing an antenna as it is directly related to the efficiency in inductive coupling. If these values are known, the Q factor and coupling coefficient can be used to calculate the exact wireless power transfer efficiency as

$$\eta = \frac{k^2 Q_1 Q_2}{\left(1+\sqrt{1+k^2 Q_1 Q_2}\right)^2} \tag{3.9}$$

While finding exact analytical solutions is difficult, estimates of these values provide reasonable design guidelines for wireless power transfer systems. For implantable devices, the sizes are severely limited, creating a low upper limit for the mutual coefficient and transfer efficiency with the primary coil antenna. Furthermore, the primary coil driver (usually a class-C or class-E amplifier) has a finite source resistance, which limits the Q factor of the primary coil antenna. To overcome these limitations, a high Q factor resonator is incorporated to increase the transfer efficiency with more positional freedom of the load coil antenna. By including an intermediate resonator, the transfer efficiency becomes the product of the efficiency between two stages of coils, which results in a higher overall transfer efficiency.

The source antenna is driven with a commercial 13.56 MHz RFID driver (Feig Electronics Inc.), which includes an automated impedance matching circuit. The intermediate resonator consists of a wire surrounding the bottom of the cage,

which acts as the resonator coil, and a capacitor to match the self-resonant frequency at 13.56 MHz. Then, the automated impedance matching feature is used to set the source parameters to maximize the transfer efficiency with the resonator loaded. Normally, the loading of the resonator onto the antenna affects the impedance seen at the source and the resonator, making it difficult to match the impedance. However, the automated impedance matching feature enables precise impedance matching of the system to utilize a resonant inductive coupling setup. Finally, the load coil, which is on the substrate of the implantable device, is implanted inside the rat and placed inside the cage.

While the load coil of the implantable device also includes an impedance matching circuit to match resonance at 13.56 MHz, the amount of current flowing to the load determines the load resistance and thus the Q factor. Nevertheless, the high Q factor of the resonator allows sufficient wireless power transfer. The power consumption of the implantable device is dominated by the μ-iLEDs, which require 19.8 mW when turned on (remaining circuit consumes <1 mW). Power transfer efficiency can be modeled using the lumped circuit model as shown in Figure 3.7, where the mutual inductance and self-inductance are found using a finite element method software (Ansys HFSS, Ansys Inc.). Measurements confirm that the implantable device in the cage receives a maximum of 38 mW at the edge of the cage and 21 mW at the center of the cage when the transmitting antenna is driven with 5 W.

3.3.2 Supercapacitor and Magnetic Shielding

To overcome angle sensitivity limitations associated with magnetic resonance coupling, two 70 mF 3.3 V commercial supercapacitors (XH414H-IV02E, Seiko Instruments) are incorporated in the circuit to act as an energy buffer. Supercapacitors are electrochemical double-layer capacitors that utilize high surface area carbon to deliver high energy densities compared to conventional capacitors. Unlike batteries, supercapacitors can be charged/discharged instantaneously, thus eliminating the current-regulating circuitry. Therefore, the received power in the load coil is converted to DC voltage using a full-bridge rectifier, which is then stepped down using a 3.2 V charge pump DC/DC voltage converter to limit overcharging of the supercapacitor. The output of the voltage converter is connected in parallel to the supercapacitor and then passed through a 3V low-dropout regulator for a steady supply voltage. Energy stored in the supercapacitor can be calculated using (3.10), to get a value of 0.72 J when charged to 3.2 V.

$$W = \int_0^Q V(q)\,\mathrm{d}q = \frac{1}{2}CV^2 \tag{3.10}$$

Since the amount of wireless power received depends on the location inside the cage, the time to charge the supercapacitor varies, but takes ~10 seconds on average and ~30 seconds in the worst case scenario. When the supercapacitors are charged to 3.2 V, they supply energy for the implantable device to operate for at least 2 minutes when the μ-iLEDs are on, without any external power. Because

the rats generally do not stay standing up more than a couple seconds, such setup was enough to reliably power the implantable device for long-term experiments. Finally, the output of the LDO is connected to the rest of the implantable device system as the low-noise power supply voltage.

The supercapacitors are encapsulated with metal, which produces eddy currents when exposed to strong magnetic fields. Eddy currents are current loops induced in a conductor by a varying magnetic field. These currents are problematic because they counteract the original magnetic field, create ohmic losses, and generate significant heat inside the conductor. Therefore, the temperature-sensitive supercapacitors need magnetic shielding to prevent eddy currents from forming. To prevent magnetic fields from reaching the supercapacitor, the fields are redirected using ferromagnetic shielding material (μ' = 150 at 13.56 MHz; 354001, Wurth Elektronik) underneath the supercapacitor. The ferrite material's low magnetic reluctance redirects the incoming magnetic fields towards the planar direction of the ferrite sheet. Because the redirected fields decrease the amount of magnetic flux flowing through the load coil, ferromagnetic material is placed only in the region underneath the supercapacitor to minimize its effect on the inductive coupling. On the other hand, the ferromagnetic material can be used to shield the entire implantable device if a layered printed circuit board is utilized, where the system is layered in the order of load coil antenna, ferrite material, and the PCB. This would allow the maximum flux flow through the load coil while shielding the circuitry from

magnetic fields. A photograph of the implantable device is shown in Figure 3.8 and the overall power circuit is shown in Figure 3.9.

3.4 Bluetooth Microcontroller

Among various wireless communication protocols, Bluetooth is one of the most convenient and flexible methods to implement in resource-constrained devices, while consuming the least amount of power. Although communication at 2.4 GHz is susceptible to absorption and scattering in biological tissue, subcutaneous implantation allows 2.4 GHz signals to be transmitted with minimal distortion. Measurements have shown that transmitting antenna power of -12 dBm from the implantable device was sufficient to reliably communicate with the iPad placed ~1 m away. An ultra-low power Bluetooth microcontroller (nRF51822, Nordic Semiconductor Inc.) is used as the main controller for the implantable device. The nRF51822 is a system on chip (SoC) that integrates 2.4 GHz radio transceiver, flash memory, ARM Cortex-M0 CPU, and various analog/digital peripherals. A precompiled Bluetooth Low Energy (BLE) protocol stack, S110 SoftDevice (Nordic Semiconductor Inc.), is programmed into the microcontroller to enable flexible and convenient BLE integration with the programmable ARM Cortex-M0. Both the microcontroller and the communication protocol operate at extremely low duty cycles (~1%), allowing the device to be in sleep mode most of the time, thus minimizing average power consumption (< 1 mW). The embedded firmware is developed with Keil Tools software (ARM Ltd.) to sample the strain sensor signal and transmit it to the iPad, allowing power-consuming computations

and signal processing to be carried out on the iPad, while the implantable device only acquires and transmits the signal.

3.4.1 Firmware Development

The Bluetooth stack contains layers that govern the communication link. First, Generic Access Profile (GAP) is the lowest layer of the Bluetooth stack which controls connections and advertising of devices. In a Bluetooth connection, a central device is the device that initiates a connection (iPad) to the resource-limited peripheral device (implantable device). The central device responds to advertising packets sent from a peripheral device with a scan response to initiate a connection. Therefore, an existing GAP profile was modified to create a unique profile for the developed closed-loop system. Next, General Attribute Profile (GATT) is the layer where actual data is transferred. The peripheral is the GATT server which holds the data to be transferred and the central is also known as the GATT client. The GATT layer includes services and characteristics which describe what kind of data will be transferred. These profiles are written in the firmware of the implantable device for the master device to recognize. For the closed-loop system, a new service profile was created to communicate using Bluetooth protocol. It includes two new characteristics that are communicated between the master and slave: strain sensor data and the LED status. The strain sensor reading characteristic contains the reading of the strain sensor and is updated by the implantable device every predefined connection interval (1 s), and the LED status characteristic is controlled by the central device which the

software controls depending on the strain sensor readings. Figure 3.10 shows a visual illustration of Bluetooth communication protocol.

Since the interval between bladder contractions is in the sub-hour range, a 1 s sampling interval is more than enough to capture the organ's activity. Therefore, the microcontroller is programed to run a one second timer using an internal RC peripheral circuit upon initiating a Bluetooth connection. Then, whenever this timer resets, an analog-to-digital interrupt handler is called to read the analog voltage from the strain sensor. Because the noise of the strain sensor measurements is dominated by motion artifacts of the rat, an internal 8-bit converter is sufficient for the conversion. The 8-bit ADC's least significant bit has a magnitude of

$$LSB = \frac{3}{2^8} = 11.7 \text{ mV} \tag{3.11}$$

which corresponds to a relatively large error margin of the ADC. This is the largest noise source of the system, but is considerably smaller than the noise generated from the motion artifacts. If the system requires a lower level of noise, an external ADC can be utilized for a higher resolution conversion and lower noise level. Following the ADC, the digital signal is stored in a TX buffer before being transmitted to the master device at the next connection interval. For the LED triggering, a general-purpose input/output pin of the microcontroller is used to switch the LED-driving transistor. Similarly, this pin can be updated at each

connection interval if the iPad transmits an update characteristic signal. Connection between the implantable device and iPad continues until it is manually disconnected by the master device or the implantable device does not receive an update for over 6 seconds (maximum supervision timeout, predetermined by Bluetooth protocol [14]).

3.5 iOS Application

The final subsystem of the closed-loop system is the custom-built iOS application. The iOS software is designed to identify abnormal conditions and trigger the μ-iLEDs by sending a signal to the implantable device. Most of the software development came after data was collected and analyzed from *in vivo* experiments, which are discussed in detail in the next chapter.

The iOS application was developed using Objective-C in Xcode by referring to a sample application provided by Nordic Semiconductor called "nRF Master Toolbox." A Cocoa plotting framework for iOS, Core Plot, was used to plot the received measurements and analyzed data on the user interface, and CoreBluetooth was used to control the communication received from the implantable device. The user interface included different measurements and tools depending on the stage of the biology experiments. Initially, the software only displayed the strain sensor readings, but the software was eventually updated such that the received data was plotted on the user interface along with the analysis of the raw signal. Moreover, the raw signal was stored in a text data file in the iPad

for further offline analysis. While a detailed investigation of the strain sensor measurement is given in the next chapter, an example strain sensor measurement of the bladder is shown in Figure 3.11. In the given measurement, the sudden decrease in resistance corresponds to the urinating points where the bladder size decreases as it voids. These timestamps, and possibly the size of these peaks, are the necessary information to analyze bladder activity. Therefore, the iOS application is programmed to collect the data from the implantable device, and use a peak finding algorithm to find these urinating timestamps. Once the software detects a voiding event, it calculates the average interval between previous voids to determine whether voids are too frequent. If the average interval falls below a certain threshold, the iPad updates the LED status characteristic to trigger the μ-LEDs in the implantable device. Detailed void detecting steps are given in the next chapter.

3.6 Device Integration

Final steps before implanting the device include integration and encapsulation of the implantable device. The PCB of the implantable base station is fabricated on a flexible PCB material (Cu/PI Pyralux, DuPont), where the layout of the PCB is defined using photolithography and etching of the copper layer. Then, after soldering components onto the PCB layout, the wires connecting the strain sensor and the μ-iLEDs are soldered onto the defined pads of the wireless base station. The base station is then encapsulated using a thin layer of epoxy followed by dip-coating with butyl and PDMS. These layers

provide a mechanically robust layer that is able to withstand biofluid penetration, while the outer PDMS layer keeps the implantable device biocompatible. The wireless base station has a long diameter of 3 cm, thickness of 1.8 mm, and weighs 420 mg. For *in vivo* experiments, the device is surgically implanted into the rat with the bladder sensor being secured using a buckle and an opening fabricated at each end of the strain sensor. The base station is then inserted between the skin and the muscle near the upper abdomen. Finally, the strain sensor measurements are recorded following ~2 days of recovery on the iPad.

3.7 Figures

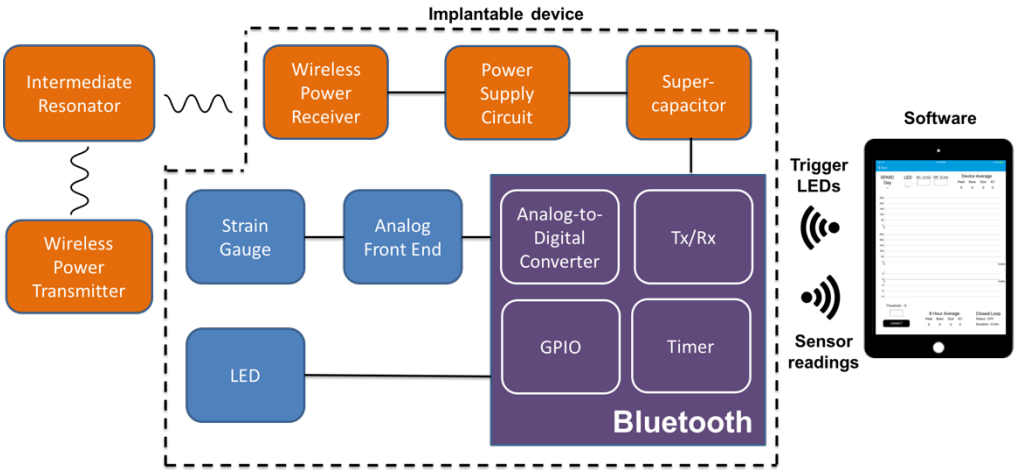

Figure 3.1: Schematic block diagram of the closed-loop system. Components are color-coded according to the four subsystems: strain sensor/μ-iLEDs (blue), powering circuit (orange), Bluetooth controller (purple), and the software (iPad).

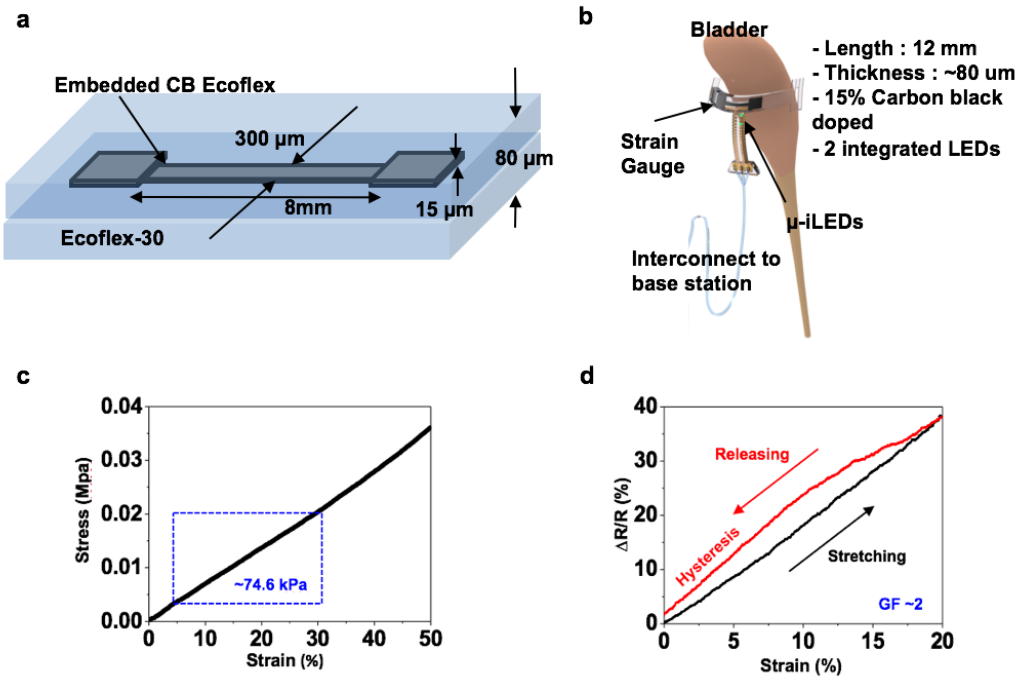

Figure 3.2: Characteristics of the strain sensor. (a) Illustration of the strain sensor including actual dimensions. (b) Illustration example of strain sensor wrapped around the bladder. (c) Stress-strain curve of the strain sensor. (d) Relative resistance change plotted against applied strain.

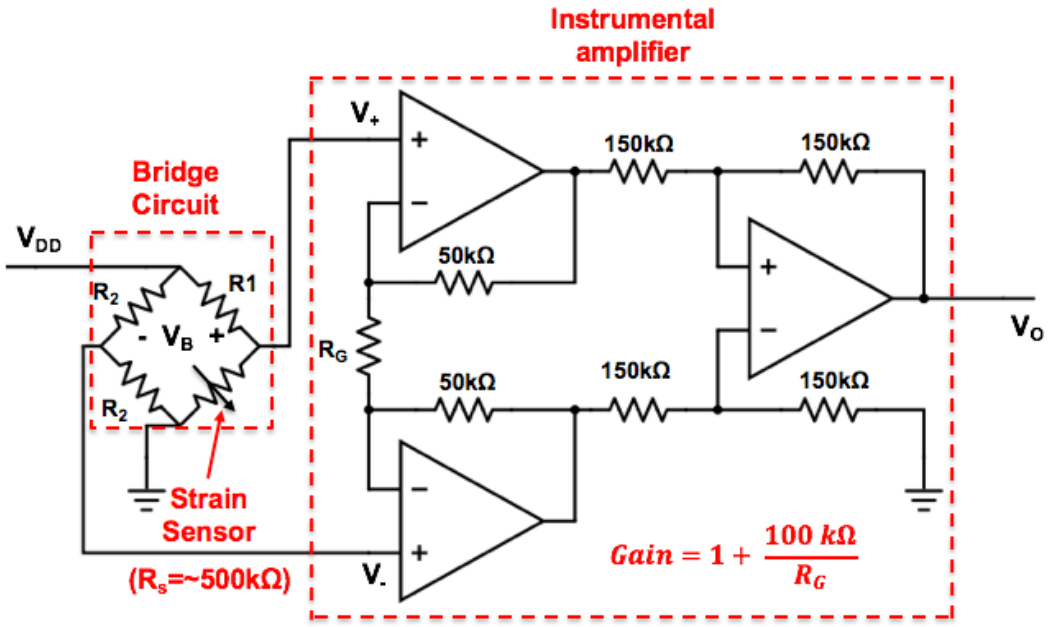

Figure 3.3: Circuit diagram of the strain sensor and analog front end. The internal circuitry of an instrumental amplifier is shown in the bigger red-dashed box, and the bridge circuit in the smaller red-dashed box. The input V_{DD} is connected from the output of the power supply circuitry, and V_O is connected to the input of the microcontroller.

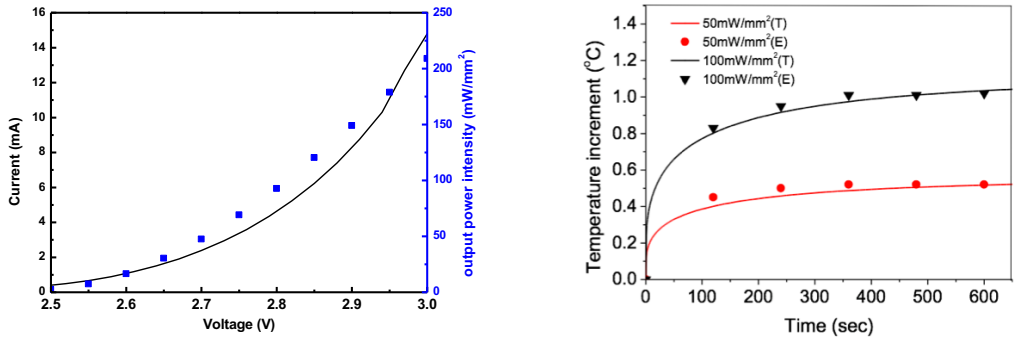

Figure 3.4: Characteristics of the μ-iLEDs. I-V curve and the corresponding measured optical power intensity (left) and theoretical/experimental temperature increment at the surface of the encapsulation at intensities of 50 mW/mm^2 and 100 mW/mm^2 (right).

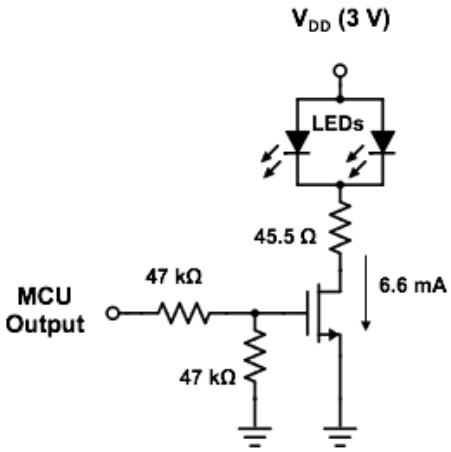

Figure 3.5: μ-iLED driver circuit. A current-limiting resistor is used to limit the current through each μ-iLED at 3.3 mA.

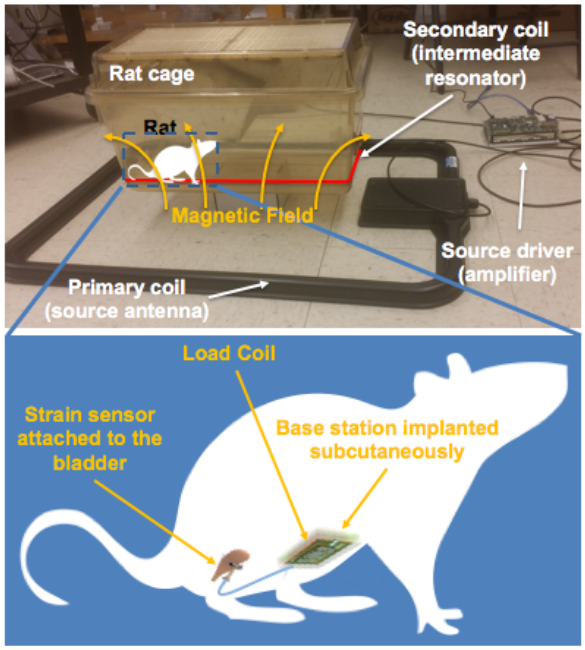

Figure 3.6: Setup overview of wireless powering (top). Illustration of device implantation inside a rat (bottom). The device is implanted subcutaneously in the abdomen such that the load coil antenna is parallel to the primary coil antenna and the intermediate resonator when the rat is standing on four legs.

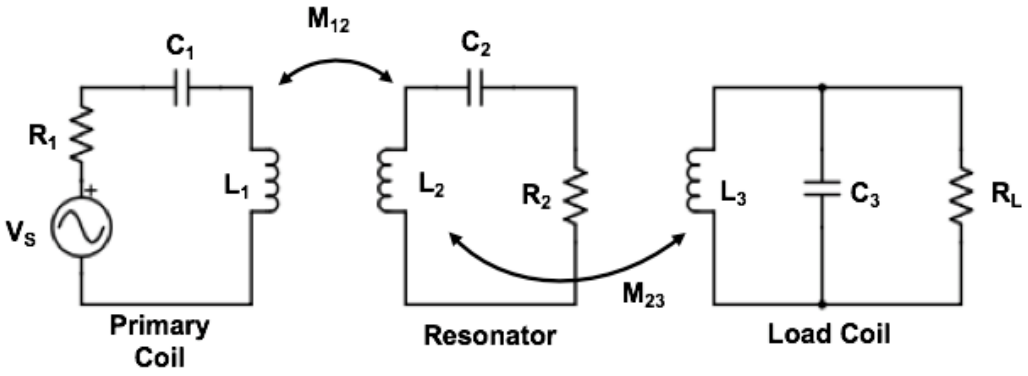

Figure 3.7: Lumped circuit model of wireless power transfer elements. Driver amplifier and the impedance matching circuit are omitted for simplicity. The inductors are a lumped representation of the loop antennas.

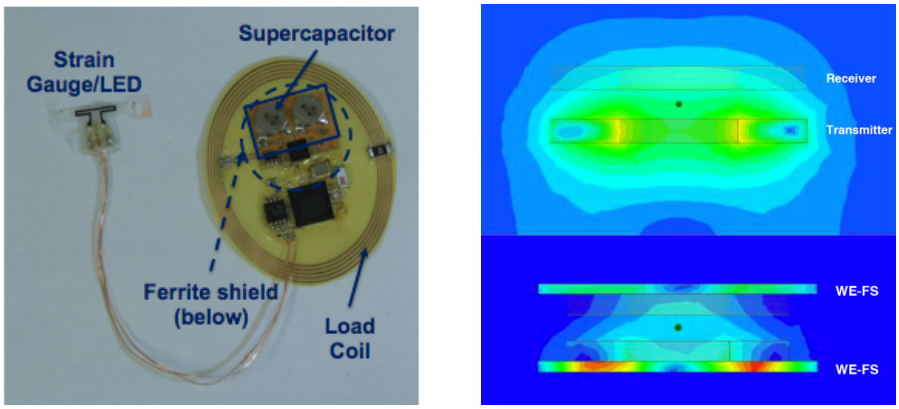

Figure 3.8: Supercapacitor and magnetic shielding. Photograph of the implantable device (left). The load coil is the antenna used for resonant inductive coupling. Effect of ferrite shield (right). An example electromagnetic simulation of H-fields being shielded with a ferrite shield. [15]

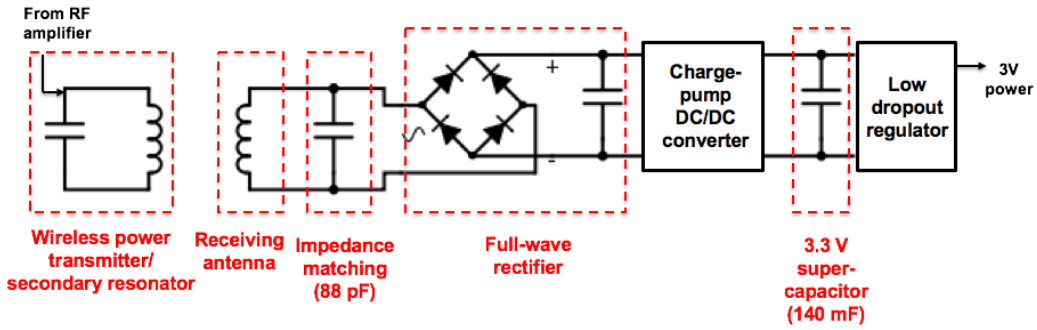

Figure 3.9: Summary of the overall powering scheme, including wireless power transfer components, impedance matching capacitor, voltage converters, and a low dropout regulator. The output of the low dropout regulator acts as the power supply voltage for the rest of the implantable device.

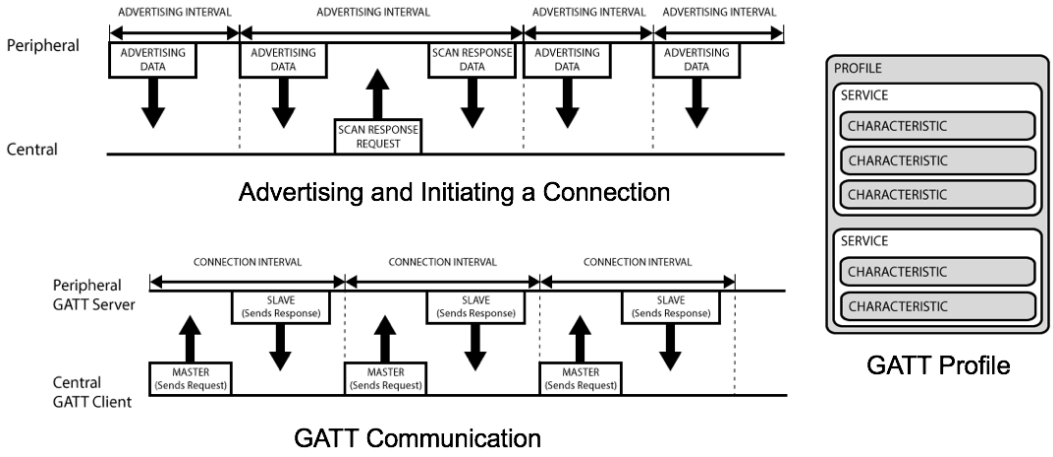

Figure 3.10: Bluetooth communication protocol. Diagram of initiating a connection, data transfer communication, and GATT profile structure [16].

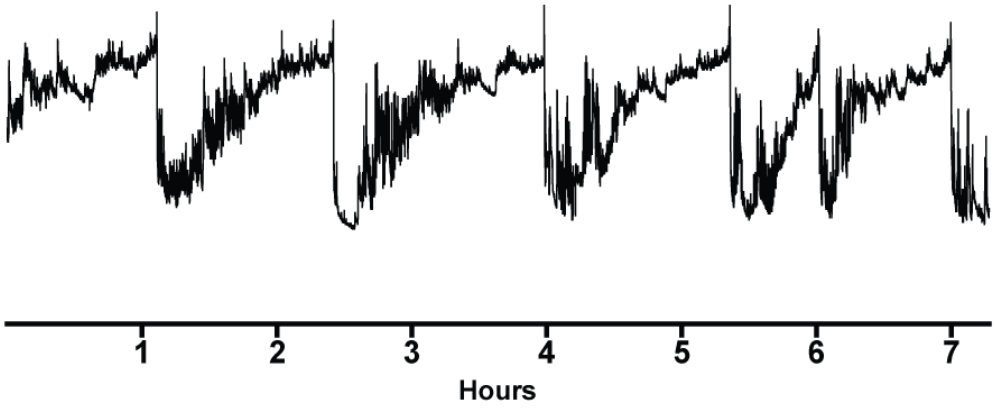

Figure 3.11: Example strain sensor measurement for 7 hours in an awake animal recorded with an iPad.

CHAPTER 4: RESULTS AND DISCUSSION

Following the development and testing phase of the implantable device, *in vivo* experiments were conducted at Washington University in St. Louis School of Medicine. The set of experiments were designed to determine the feasibility of using these strain sensors to monitor bladder activity for rats. Then, tests were conducted to see if the device was capable of activating optogenetic proteins for neuromodulation. Finally, based on the collected *in vivo* data, parameters for the closed-loop system were established. The conditional neuromodulation shown here is a preliminary result and research is ongoing to refine the closed-loop system with a higher level of accuracy and consistency.

4.1 Strain Sensor and Optogenetics

After the strain sensor was developed and tested *in vitro*, pressure measurements and strain sensor measurements on anesthetized rats were compared side by side to observe the correlation. The goal of the experiments was to verify the feasibility of the strain sensor as an alternative to the pressure measurements and prove that the strain sensor did not constrict the bladder's natural behavior. An example comparison of the two measurements is shown in Figure 4.1. As shown in the figure, the resistance measurement very closely resembles the pressure inside the bladder, confirming the strain sensor's utility in monitoring the bladder activity. One unexpected challenge was that the exact location of the strain sensor significantly altered the amount of change in

resistance applied on the strain sensor. Another important observation with the measurements was that the strain sensors were able to detect non-voiding contractions of the bladder, which are not detectable using metabolic cages. This demonstrated that the strain sensor can measure the bladder activity as well as the pressure transducers, but in a less invasive method. Moreover, cystometry experiments on the same rats with and without the strain sensor verified that the strain sensor did not constrict the bladder's natural movements. On the other hand, the slippery biofluids on the rats' bladder made it difficult for the strain sensor to always stay in the same position for some experiments. Thus, further research is ongoing to develop a mechanism to keep the strain sensor fixed at a particular position. Otherwise, the strain sensor proved to be a promising method of measuring bladder activity.

Then, optogenetics experiments were conducted to test if the developed device was able to activate the optogenetic proteins. The main goals of these closed-loop systems were to identify overactive bladder activity and help alleviate the conditions by delaying contraction intervals. Figure 4.2 shows an example measurement of an optogenetic experiment on anesthetized rats. A comparison between a control rat and a transgenic rat offers evidence of optogenetics as a method to delay contractions. The contraction interval increased ~20% for the transgenic rats when the LEDs were on, while no changes were observed on the control rat.

4.2 Void Identification

After the initial experiments verified the feasibility of these devices, many iterations of *in vivo* experiments were carried out to collect strain sensor measurements in awake animals. In parallel, the rats were placed in metabolic cages which have an integrated scale that monitors the voiding events. By comparing the strain sensor measurements to the metabolic cage data, a method to identify the voiding events was developed. Because the strain sensor is very sensitive to mechanical contact, results demonstrated that the motion artifacts were a very big source of noise. However, the voiding events were clearly distinguishable with sudden drops in the resistance despite the noise. An example measurement in an awake rat is shown in Figure 4.3a.

To find an automated void identification method, various data analyses with large sets of strain sensor data were conducted. A simple method that resulted in an accurate algorithm included using a 120-point moving average filter, down-sampling, and calculating the derivative. First, the moving average filter removes most of the motion artifacts and higher frequency noise. Next, because the contractions following a voiding event take about 1 minute, the signal is down-sampled to 1 sample/min. Then, the derivative of the 1 sample/min data highlights the voiding event with a large negative slope. Then, when the derivative falls below the preset threshold of 10 units/s (determined from experiments), the software determines that a voiding cycle has occurred and records it.

4.3 Closed-loop System

The final step in the biology experiments was to demonstrate the possibility of the closed-loop system. A virus was introduced to rats to cause cyclophosphamide (CYP)-induced cystitis, which is a temporary condition that increases the voiding frequency. It was observed that normal rats urinate about once every hour, and the rats with cystitis urinate two to three time times every hour during the daytime. Therefore, the first preliminary closed-loop parameters were established by defining a threshold contraction interval. Every time voiding events are recorded in the software, the software recalls three recent voiding timestamps to calculate the average contraction interval. When the voiding frequency exceeds 1.5/hour, the software sends a signal to turn on the LEDs to inhibit bladder function, and increase the contraction intervals. While the initial parameters were set and simulated using Matlab to test its functionality, the entire closed-loop *in vivo* experiments have not yet been conducted. However, most of the supporting experiments and simulations have been successful, and simulations with real measurements have shown conditional triggering at the correct times. Further research is ongoing to determine a refined algorithm to better differentiate between normal and abnormal bladder behavior, which will allow a more precise control of the bladder function using optogenetics. An example comparison controlled inhibition of the bladder is shown in Figure 4.4.

4.4 Figures

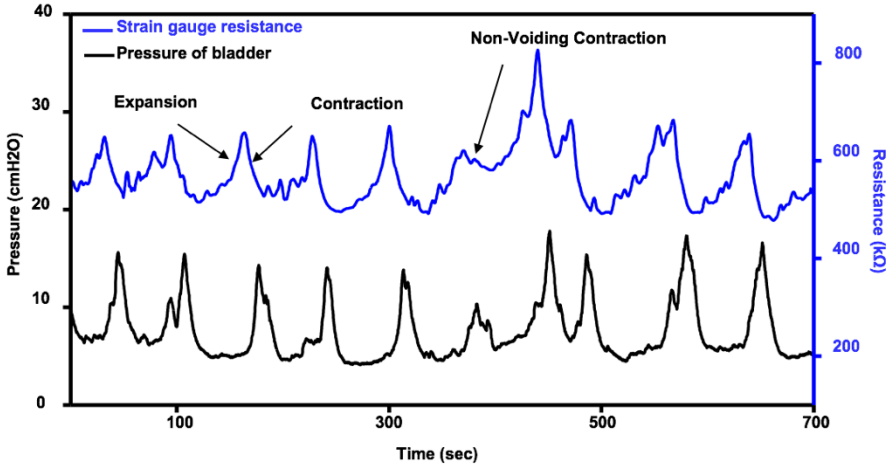

Figure 4.1: Comparison of strain sensor measurement and pressure measurement of the bladder on an anesthetized rat. The strain sensor measurement is very closely correlated to the pressure measurement, confirming the feasibility of using the strain sensors to monitor bladder activity.

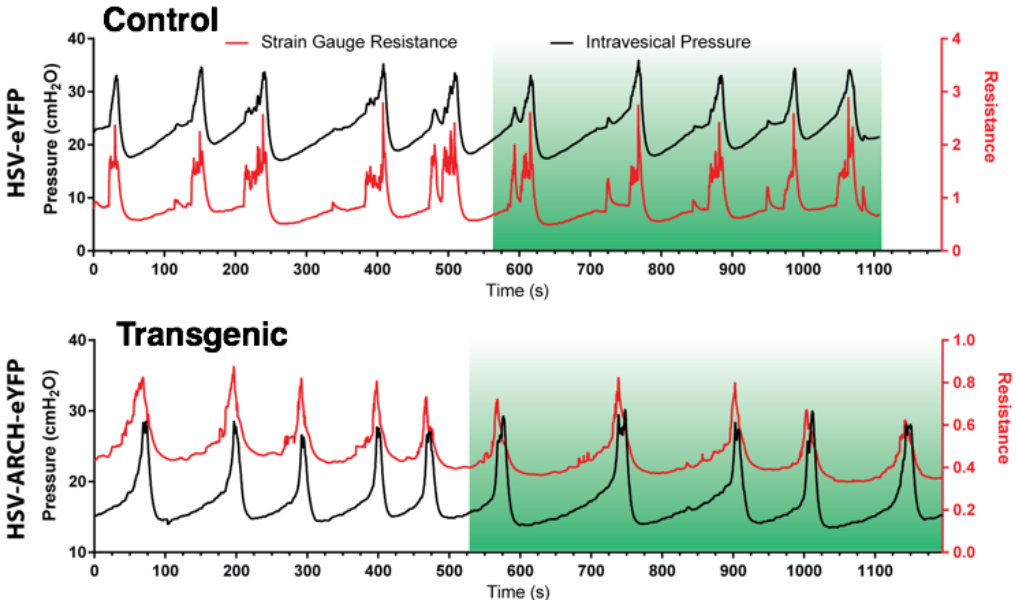

Figure 4.2: Example measurements during an anesthetized optogenetic experiment for a control and transgenic rat. The green region corresponds to the time the LED is on. Note that the contraction interval increases when the LED is on.

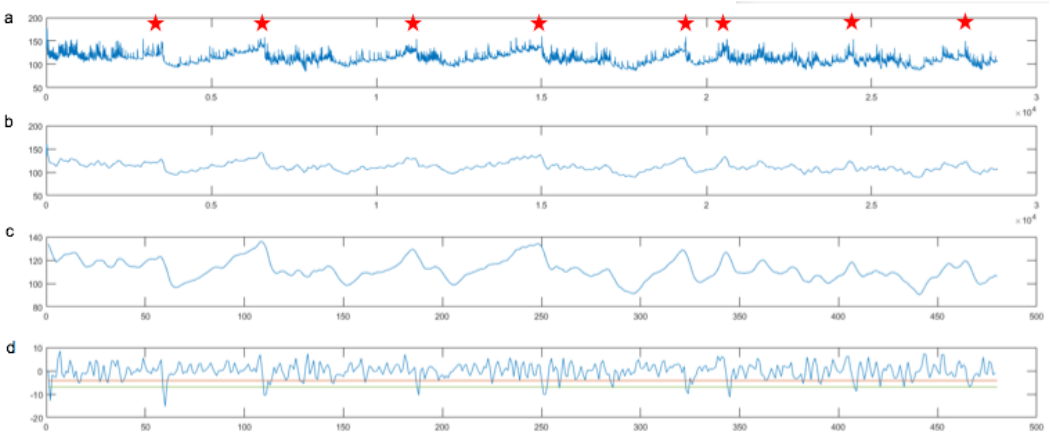

Figure 4.3: Step-by-step analysis of peak identification algorithm. (a) Raw data collected wirelessly from implanted strain sensor. (b) 150-point moving average filtered data. (c) Down-sampled to point per 60 samples. (d) Derivative of the down-sampled data. The detected voids by the software are marked in red stars in (a).

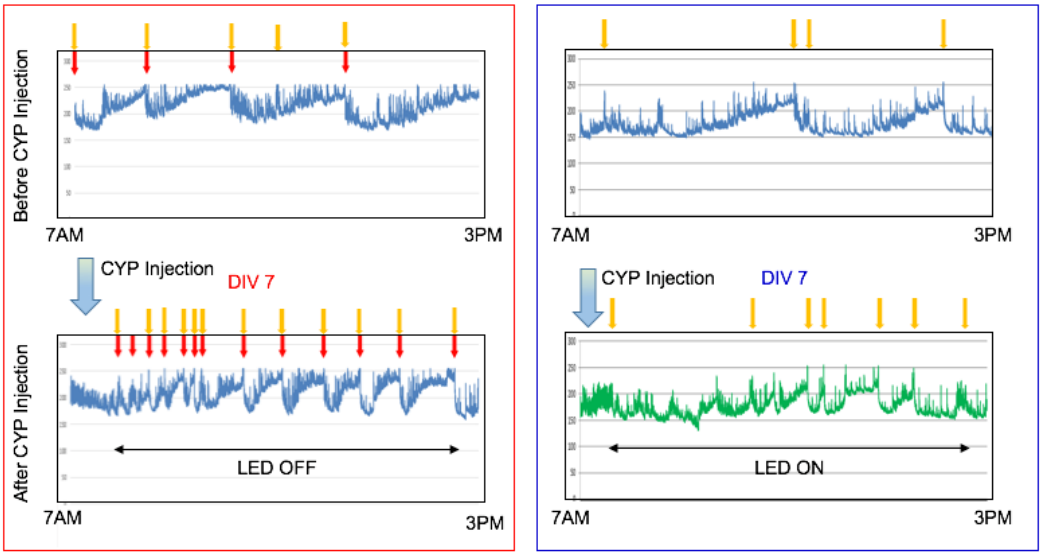

Figure 4.4: Comparison of CYP rats' bladder activity with and without optogenetics. The plots show strain sensor recordings during the day. The red box shows the strain sensor measurement of a rat where optogenetics was not triggered. In the blue box, optogenetics is triggered manually. With the LED on, it can be seen that the contraction intervals are not as short as the ones on the left. The yellow arrows correspond to voids detected by the software and the red arrow corresponds to confirmed voids from the metabolic cage.

CHAPTER 5: CONCLUSION

This thesis introduces an implantable device that is capable of conditionally inhibiting bladder activity to potentially help alleviate abnormal bladder conditions. The iOS software included in the system is to conveniently analyze data and control parameters during biology experiments. With more experimental data, it would be possible to embed the closed-loop algorithm into the implantable device firmware and remove the need for wireless communication with a user interface. Then, like a pacemaker, the device would be implanted for continuous monitoring and consistent treatments in a non-hospital environment. Moreover, the developed strain sensor shows potential to be used as an alternative bladder measurement method, which is much less invasive than the pressure measurement. Since this research is in its beginning stage, there are various areas that can be improved.

5.1 Future Work

Many choices in the design of this closed-loop system were made out of convenience in order to simplify and accelerate the design process. Therefore, there is room to significantly improve the performance of the device, while further miniaturizing it. Designing an application-specific integrated circuit (ASIC) would be a time-extensive process, but could significantly minimize the device dimension and power consumption. With more *in vivo* data, a refined algorithm can be designed and built into the ASIC such that an external software

and user interface is not necessary. Moreover, if the signal needs to be acquired wirelessly, the communication protocol and radio telemetry can be custom built to minimize power consumption at a frequency less susceptible to absorption/scattering in biological tissues. Such optimizations can decrease the power to a μW range, which can decrease the size of the wireless power receiving antenna. However, wireless powering will be more challenging with larger animals due to its angle sensitivity and larger antenna dimension mismatch. A possible solution would be to build the implantable device with batteries and a wireless charging circuit to charge the batteries during inactivity. Also, additional sensors can be utilized near the strain sensor to differentiate motion artifacts from the strain sensor signal. Finally, research is ongoing to improve the mechanics of the device encapsulation to make the device more compliant in a physiological setting.

5.2 Future Research Directions

The next step in research is to utilize the system to help further understand the bladder function and expand it for larger animals. While the strain sensor developed here is in a band geometry to fit experiments with rat bladders, similar strain sensors with different geometries can be developed to fit experiments for larger animals and potentially humans. Assuming a similar approach is possible, it will not only eliminate the need to use invasive pressure catheters or nerve interfacing electrodes for bladder measurements, but also provide a unique method to study the bladder function. Next, further optogenetics experiments will

help advance the neuromodulation methods to help alleviate bladder conditions. Although optogenetics is a relatively new technique, ongoing human trials prove that the technique is promising for clinical applications as well [17]. Finally, by utilizing the versatile Bluetooth platform (or ASIC), the system can be easily modified to incorporate different types of sensors (electrical recording or pressure) and actuators (electrical stimulation or microfluidic drug delivery) for a more sophisticated closed-loop system interfacing different organs.

REFERENCES

[1] Joung, Y. (2013). Development of Implantable Medical Devices: From an Engineering Perspective. *International Neurourology Journal*, 17(3), p.98.

[2] Irwin, D., Milsom, I., Hunskaar, S., Reilly, K., Kopp, Z., Herschorn, S., Coyne, K., Kelleher, C., Hampel, C., Artibani, W. and Abrams, P. (2006). Population-Based Survey of Urinary Incontinence, Overactive Bladder, and Other Lower Urinary Tract Symptoms in Five Countries: Results of the EPIC Study. *European Urology*, 50(6), pp.1306-1315.

[3] Fitzpatrick, M. (2008). Sacral nerve stimulation for treatment of refractory urinary urge incontinence: A review. *British Journal of Neuroscience Nursing*, 4(7), pp.322-325.

[4] Rajagopalan, S., Sawan, M., Ghafar-Zadeh, E., Savadogo, O. and Chodavarapu, V. (2008). A Polypyrrole-based Strain Sensor Dedicated to Measure Bladder Volume in Patients with Urinary Dysfunction. *Sensors*, 8(8), pp.5081-5095.

[5] Majerus, S., Garverick, S., Suster, M., Fletter, P. and Damaser, M. (2012). Wireless, Ultra-Low-Power Implantable Sensor for Chronic Bladder Pressure Monitoring. *ACM Journal on Emerging Technologies in Computing Systems*, 8(2), pp.1-13.

[6] Dakurah, M., Koo, C., Choi, W. and Joung, Y. (2015). Implantable Bladder Sensors: A Methodological Review. *International Neurourology Journal*, 19(3), pp.133-141.

[7] Gutierrez, C. and Meng, E. (2010). Low-cost carbon thick-film strain sensors for implantable applications. *Journal of Micromechanics and Microengineering*, 20(9), p.095028.

[8] Deisseroth, K., Feng, G., Majewska, A., Miesenbock, G., Ting, A. and Schnitzer, M. (2006). Next-Generation Optical Technologies for Illuminating Genetically Targeted Brain Circuits. *Journal of Neuroscience*, 26(41), pp.10380-10386.

[9] Park, S., Brenner, D., Shin, G., Morgan, C., Copits, B., Chung, H., Pullen, M., Noh, K., Davidson, S., Oh, S., Yoon, J., Jang, K., Samineni, V., Norman, M., Grajales-Reyes, J., Vogt, S., Sundaram, S., Wilson, K., Ha, J., Xu, R., Pan, T., Kim, T., Huang, Y., Montana, M., Golden, J., Bruchas, M., Gereau, R. and Rogers, J. (2015). Soft, stretchable, fully implantable miniaturized optoelectronic systems for wireless optogenetics. *Nature Biotechnology*, 33(12), pp.1280-1286.

[10] Li, C., Guan, G., Zhang, F., Song, S., Wang, R., Huang, Z. and Nabi, G. (2014). Quantitative elasticity measurement of urinary bladder wall using laser-induced surface acoustic waves. *Biomedical Optics Express*, 5(12), p.4313.

[11] A Designer's Guide to Instrumental Amplifiers. (2006). 3rd ed. [ebook] Available at: http://www.analog.com/en/education/education-library/dh-designers-guide-to-instrumentation-amps.html [Accessed 15 Jul. 2017].

[12] Mohanty, S. and Lakshminarayananan, V. (2015). Optical techniques in optogenetics. *Journal of Modern Optics*, 62(12), pp.949-970.

[13] Lu, X., Wang, P., Niyato, D., Kim, D. and Han, Z. (2016). Wireless Charging Technologies: Fundamentals, Standards, and Network Applications. *IEEE Communications Surveys & Tutorials*, 18(2), pp.1413-1452.

[14] Bluetooth Core Specification. (2016). 5th ed. [ebook] p.748. Available at: https://www.bluetooth.com/specifications/adopted-specifications [Accessed 15 Jul. 2017].

[15] Application Note: Going Wireless with Magnetic Shielding. (2013). [ebook] Jorge Victoria Ahuir, pp.4-5. Available at: http://www.we-online.com/web/fr/electronic_components/produkte_pb/application_notes/funkproduktеflexibelgeschirmt.php [Accessed 17 Jul. 2017].

[16] Learn.adafruit.com. (2015). *Introduction | Introduction to Bluetooth Low Energy | Adafruit Learning System*. [online] Available at: https://learn.adafruit.com/introduction-to-bluetooth-low-energy?view=all [Accessed 17 Jul. 2017].

[17] Nature (2016). Light-controlled genes and neurons poised for clinical trials. [online] Available at: http://www.nature.com/news/light-controlled-genes-and-neurons-poised-for-clinical-trials-1.19886 [Accessed 17 Jul. 2017].